Calibration of interferometric SAR images

Jan O. Hagberg and Lars M.H. Ulander

Department of Radio and Space Science
Chalmers University of Technology
S-412 96 Göteborg, Sweden

ABSTRACT

Well calibrated data products are important to support advanced SAR applications. In the past, robust methods have been developed to perform radiometric calibration of SAR intensity images. A problem over land is that the SAR radiometry is affected by topography and information about the local surface slope is required for retrieving the backscattering coefficient. Repeat-pass SAR interferometry has the potential of providing the necessary information. Local surface slope maps may be directly generated from the instantaneous frequency in the complex interferogram, and no phase unwrapping is required. The slope maps may also be used as input to backscattering models for additional normalisation of the image power. We show results from applying the algorithms to an ERS-1 SAR interferogram over Sardinia. The degree of coherence is another data product which may be derived from the SAR interferogram and has a potential for classification of surface type. We discuss coherence estimation and various effects which will bias the estimate. It is shown that image registration, resampling effects and uncompensated topography decrease the estimate whereas the limited estimation window size increases the estimate. Accurate coherence calibration thus requires corrections for these effects.

1. INTRODUCTION

Across-track SAR interferometry is a technique which provides measurements of topography [1]. The technique combines two complex SAR images, an interferometric pair, taken over the same area but from two slightly separated across track positions. It requires that the degree of coherence between the two images is sufficiently high to allow two-dimensional unwrapping of the interferogram phase to generate a digital elevation model (DEM) over the area. Once the DEM is available, it is straight forward to produce slope maps. However, temporal decorrelation affects a repeat-pass system like ERS-1 and the degree of coherence is therefore often too low for conventional phase unwrapping.

In this paper, we retrieve surface slope and radiometric calibration corrections directly from the interferogram phase, without phase unwrapping. We use an approach where the surface normal is parameterised in two spherical angles. The method operates in the slant range geometry and it is based on instantaneous frequency estimation using a short-time FFT in the interferogram. Explicit and simple equations relate the instantaneous frequency with the slope parameters. Slope estimation based on estimation of the interferogram phase differences has been discussed in [2], but this method is not useful when the signal-to-noise ratio is low. A method based on the difference in unwrapped interferometric height has also been used in [3]. These methods are applied in ground range geometry and thus requires an additional coordinate transformation.

Surface slope maps have many other applications such as estimation of drainage basins in hydrology or hydrochemistry as well as for soil erosion modelling. Accurate slope information is also useful as input to backscattering models, for coherence estimation and as additional information to improve the phase unwrapping.

2. TERRAIN SLOPE

A complex interferogram is formed by multiplication of one image with the complex conjugate of the other image, followed by procedures to optimise the fringe visibility. The differential of the interferogram phase, $d\Phi$, is related

Keywords: SAR, interferometry, calibration, radiometry, slope, coherence

to the differential of the terrain altitude dz according to (see figure 1)

$$d\Phi = \frac{4\pi B_n}{\lambda R} \cdot \left(\frac{dR}{\tan\theta} + \frac{dz}{\sin\theta}\right) = C \cdot \left(\frac{dR}{\tan\theta} + \frac{dz}{\sin\theta}\right) \quad (1)$$

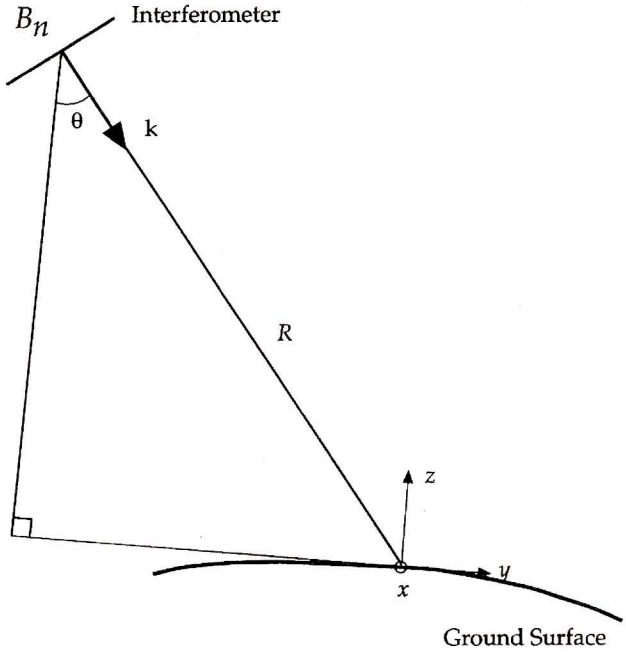

Figure 1 - Interferometric SAR system geometry.

where B_n is the interferometric baseline perpendicular to the line-of-sight, λ is the radar wavelength, R is the slant range, and θ is the incidence angle for a horizontal surface. The surface normal vector which defines the surface orientation can be parameterised by two spherical angles u and v, representing the slope angle and the direction of the slope, respectively (see figure 2). It can be shown that these angles may be determined from the interferogram phase derivatives as [4]

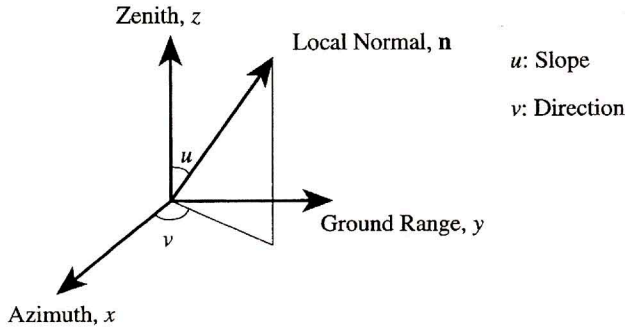

Figure 2 - Two spherical angles u *and* v *defines the surface orientation.*

$$\tan v = \sin\theta \frac{\left(\Phi'_R - \frac{C}{\tan\theta}\right)}{\Phi'_x}$$

$$\tan u = \frac{\sqrt{(\Phi'_x)^2 + \left(\sin\theta\left(\Phi'_R - \frac{C}{\tan\theta}\right)\right)^2}}{\frac{C}{\sin\theta} + \cos\theta\left(\Phi'_R - \frac{C}{\tan\theta}\right)} \quad (2)$$

The interferogram phase derivatives Φ'_x and Φ'_R are directly related to the instantaneous frequency in azimuth (f_x) and in slant range (f_R) as

$$d\Phi = \Phi'_x dx + \Phi'_R dR = 2\pi \cdot (f_x dx + f_R dR) \quad (3)$$

Similar expressions have also been derived for the modified interferogram phase, that is when the phase is compensated for the expected phase variation for a horizontal plane [4].

3. RADIOMETRIC CALIBRATION

Radiometric calibration establishes the relation between the image intensity and the backscattering coefficient for an area of interest. In recent years, calibration techniques have been developed where the calibration accuracy is better than ±1 dB over flat areas. However, problem still remains over sloping terrain since a correction for surface orientation requires surface slope information.

If the calibration constant (σ/E) is known, the backscattering coefficient σ^0 may be determined from the SAR calibration equation

$$\sigma^0 = \left(\frac{\sigma}{E}\right) \cdot \rho \cdot \frac{dA_R}{dA_g} \quad (4)$$

where P is the mean image power (noise subtracted) and dA_R and dA_g are corresponding area elements in the SAR image and on the ground, respectively. The calibration constant can be determined from a reference point target [5, 6]. The area projection factor is usually known and constant over flat terrain, but varies with terrain slope over mountainous areas and a slope map is therefore required to perform the radiometric calibration. The geometrical projection factor may also directly be estimated from the interferogram phase derivatives in the original slant range representation according to [4]

$$\frac{dA_g}{dA_R} = \sqrt{1 + \frac{\Phi'^2_R + \Phi'^2_x}{C^2}} \tag{5}$$

Once the local incidence angle is known, appropriate models for the backscattering coefficient as a function of the polarisation state, incidence angle and aspect angle may be used to perform additional corrections.

4. ESTIMATION OF INSTANTANEOUS FREQUENCY

Several signal processing techniques have been suggested for estimation of the instantaneous frequency of an analytical signal (see [7] for a recent review). We have used an algorithm based on interpolation of the peak of the two-dimensional short-time FFT to estimate the instantaneous frequencies. This estimate is equivalent to the ML estimate of the frequency of a complex sinusoid imbedded in stationary complex Gaussian white noise. The typical size of the estimation window that we used in an ERS-1 interferogram is 4 x 20 pixels. The interpolation is performed by an initial zero-padding to 64 x 64 or 128 x 128 pixels followed by a second order polynomial interpolation of the peak in the Fourier domain. The RMS error for the estimate is close to the Cramer-Rao bound above a SNR threshold [8]

$$RMS\left(\hat{f}\right) = \frac{\sqrt{6}}{2\pi} \cdot \frac{1}{\sqrt{SNR \cdot N_L^3}} \tag{6}$$

where N_L is the number of independent samples and SNR is related to the degree of coherence, $|\gamma|$, according to

$$SNR = \frac{|\gamma|}{1 - |\gamma|} \tag{7}$$

The method performs satisfactory over moderate slopes but is limited by ambiguities for large slopes, especially for areas sloping towards the radar. The maximum unambiguous surface slope angle, u_{max}, in the slant range direction depends on the interferometric baseline and is set by the Nyquist limit

$$\tan\left(\theta - u_{max}\right) = \frac{\rho_R C}{2\pi} \tag{8}$$

where ρ_R is the slant range resolution. Eq. (8) is illustrated in figure 3 for $C = 0.036$ and $\theta = 23°$.

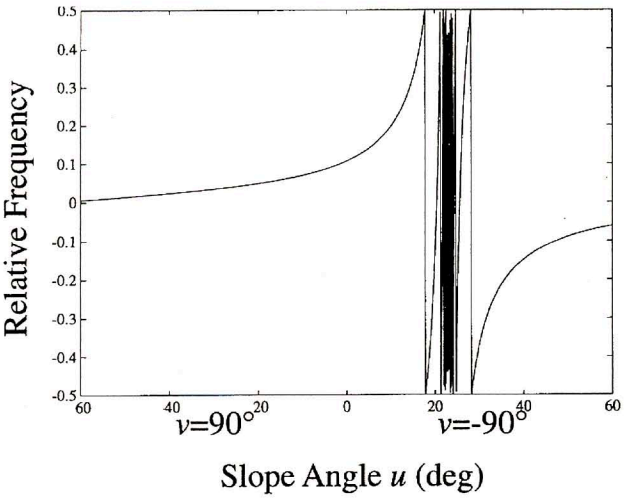

Figure 3 - Slant range interferogram frequency versus incidence angle for $C = 0.036$ m^{-1} and $\theta = 23°$. The frequency is scaled so that 0.5 corresponds to the Nyquist frequency.

5. RESULTS FROM SARDINIA

The algorithms for slope estimation and radiometric calibration correction over topographic terrain has been tested on the ERS-1 SAR interferometric reference data set, with a baseline of 138 m. An area (16 x 3 km^2) at the east coast of Sardinia was selected. A sliding window of 4 x 20 pixels, padded with zeros to 64 x 64 pixels, was used to calculate the short-time FFT, from which the slope was estimated.

The original intensity image, the corresponding geometrical projection factor and the calibrated σ^0-image are presented in figures 4a, b and c. Note that almost all intensity variations in this case are due to geometrical effects. The flat earth compensated interferogram phase and the slope angles u and v are presented in figures 5a, b and c. Flat areas ($u \approx 0°$) are marked with blue colour and areas where we get ambiguous results are marked with red colour in figure 5b. Mountain valleys and ridges are very easy to identify by looking at the slope direction in figure 5c.

6. ESTIMATION OF COHERENCE

The coherence is defined as [9]

$$\gamma = \frac{E\left[g_1 g_2^*\right]}{\sqrt{E\left[|g_1|^2\right] E\left[|g_2|^2\right]}} \tag{9}$$

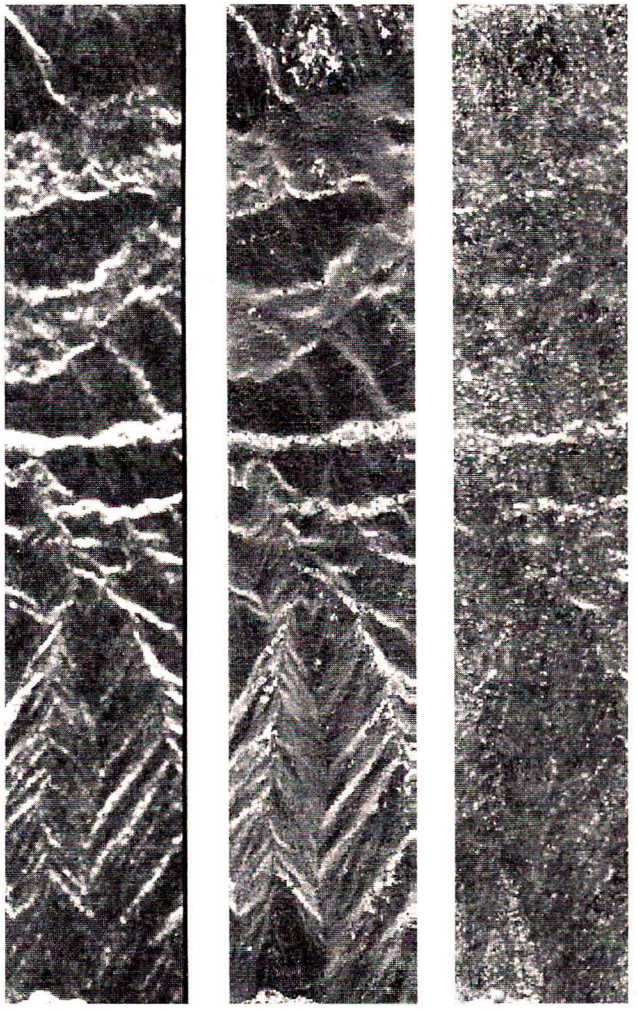

Figure 4 - a/ Original intensity image over Sardinia.
b/ Radiometric correction coefficient derived from interferogram.
c/ Calibrated σ^0 image.

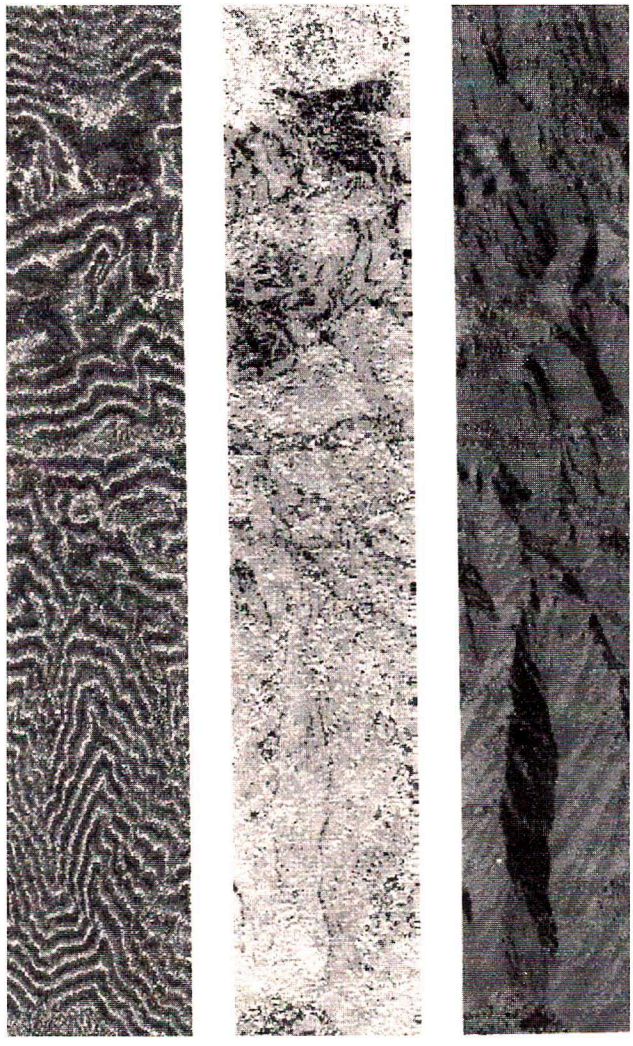

Figure 5 - a/ Flat earth compensated interferogram over Sardinia.
b/ Slope angle, u, *derived from interferogram. The red colour corresponds to ambiguous slope angles, and the blue colour to slope angles between 0° and 7°.*
c/ Slope direction, v, *derived from interferogram. The colour wheel is defined from blue (v = ±180°) over red (v = -60°) and green (v = 60°) to blue again.*

See plate III at end of volume

where g_1 and g_2 are the complex pixel values, and $E[\cdot]$ is the ensemble average operator. The degree of coherence between two images mainly depends on three factors; thermal noise, spatial decorrelation and temporal decorrelation [10]. Image registration and interpolation of one single look complex image must be performed carefully in order to preserve the degree of coherence between the images.

Assuming ergodicity, we may estimate the degree of coherence by spatial averaging according to [11]

$$|\gamma| = \frac{\left|\sum^{N} g_1 g_2^{*} e^{-j\varphi(x,R)}\right|}{\sqrt{\sum^{N} |g_1|^2 \sum^{N} |g_2|^2}} \qquad (10)$$

where the summation is over N pixels and $\varphi(x,R)$ is used to compensate for the phase changes due to topography. The estimate is asymptotically unbiased for large N if $\varphi(x,R)$ is correct. The most accurate way to perform the geometric compensation would be to use a DEM. However, often no such map exists, and a simpler procedure is then to assume the surface to be a tilted plane. The degree of coherence may then be estimated from the peak magnitude of the Fourier transform according to

$$|\gamma| = \frac{\left|\sum^{N} g_1 g_2^{*} e^{-j2\pi(f_x x + f_R R)}\right|_{\max}}{\sqrt{\sum^{N} |g_1|^2 \sum^{N} |g_2|^2}} \qquad (11)$$

where the maximisation is performed over f_x and f_R. The latter method works well if the area is smooth and if we use reasonably small areas in the FFT. However, any uncompensated topography will decrease the coherence. It is possible to estimate this effect by assuming the deviation from a tilted plane to be Gaussian distributed (variance σ_h^2). We then get an extra decorrelation factor that is due to uncompensated topography according to [11]

$$|\widehat{\gamma}| = |\gamma| \cdot e^{-\frac{1}{2}\left(\frac{4\pi B_n}{\lambda R \sin\theta}\sigma_h\right)^2} \qquad (12)$$

In order to conserve the degree of coherence it is also important that the interpolation is carefully performed. The effect of the interpolator has been studied by generating several offsets for an ERS-1 SLC image by using a long sinc-interpolator and resample it back again by using different two-dimensional interpolators. The degree of coherence between the output image from the interpolators and the original image was measured according to Eq. (10) using a 4 x 16 window. The results are plotted for different starting offsets in figure 6. A cubic interpolator will decrease the degree of coherence about 2% which should be good enough for most applications. The more time consuming sinc-interpolators perform even better.

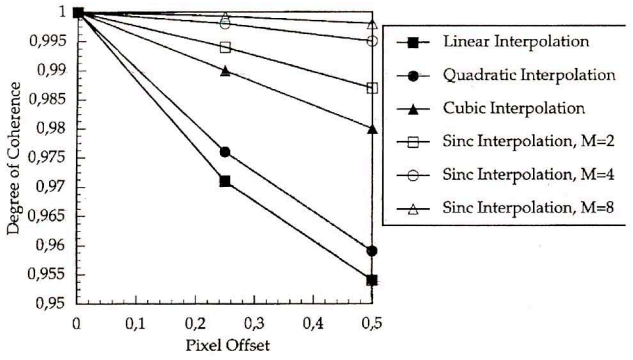

Figure 6 - Degradation of the degree of coherence for different interpolators. Equal starting pixel offset was used in both range and azimuth. Pixel offset = 0.5 therefore represents the worst case. (2M + 1 is the number of coefficients in the sinc-interpolator).

The effect of image registration accuracy and averaging window size, N, has been studied by measuring the average degree of coherence as a function of image offset, normalised to the resolution, for one ERS-1 SLC image. The theoretical degree of coherence as a function of image offset for the ERS-1 SAR is slightly different than for a sinc-type impulse response due to spectral windowing. Figure 7 shows that the image registration must be better than 1/8 resolution cell in order to keep the loss of coherence below 3%. It also indicates that the estimated degree of coherence is biased for small averaging windows at low coherence. The bias effect is also illustrated in figure 8a where the average value for the estimated degree of coherence between two images is plotted for different number of independent samples, N_L. The corresponding standard deviation of the degree of coherence estimate are plotted in figure 8b. The local imaging geometry was assumed to be known in both figure 7 and 8 ($f_x = f_R = 0$), hence only the interferogram phase was estimated from the data. If the instantaneous frequencies must be estimated from the data as well, the bias effect will increase. Smaller window sizes are preferred for coherence estimation due to higher resolution and less deviation from a tilted plane. However, this implies that the bias as well as the standard deviation increase. Our results suggest that the bias may be corrected, at least when the slope is known.

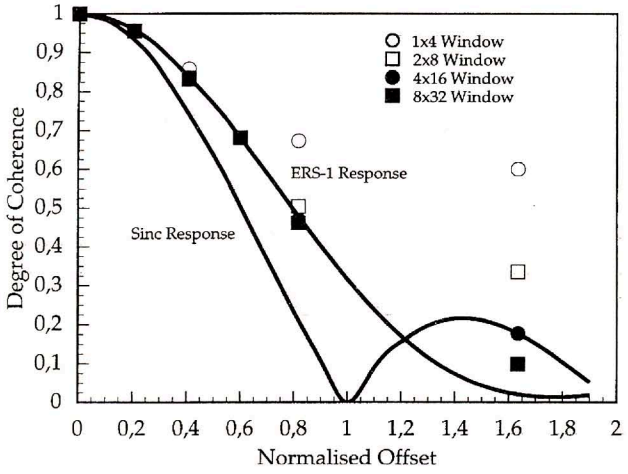

Figure 7 - Average degree of coherence as a function of image offset normalised to the radar resolution. It was measured for different window sizes. The solid lines represents the theoretical values for a sinc impulse response and the ERS-1 SAR impulse response, respectively.

7. CONCLUSIONS

In this paper, we have shown that SAR interferograms can be used for surface slope estimation and radiometric calibration correction over sloping terrain. The method was applied to an ERS-1 SAR interferogram over Sardinia. Our algorithm works in the slant range geometry and is based on instantaneous frequency estimation in the interferogram, therefore no initial phase unwrapping is required. The short-time FFT is used to estimate the frequency. It performs satisfactory, although ambiguities may distort the result for large surface slope angles. More sophisticated algorithms, for example the cross Wigner-Ville distribu-

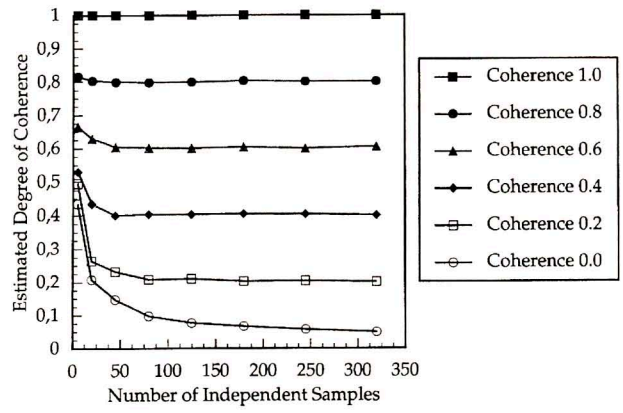

(a)

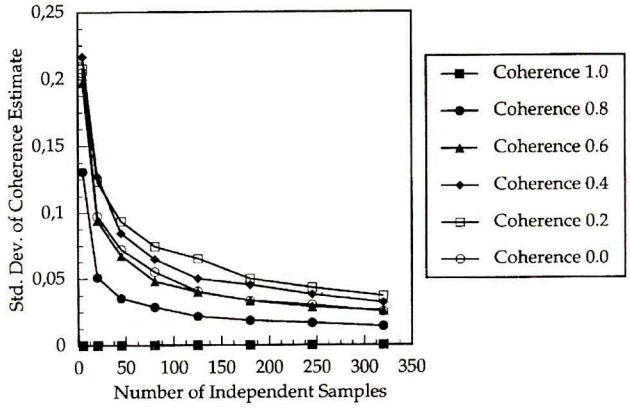

(b)

Figure 8 - a/ Estimated degree of coherence versus number of independent samples, N_L, in the averaging window for different degree of coherence.
b/ Corresponding standard deviation of estimated degree of coherence versus number of independent samples, N_L, in the averaging window.

tion, may be necessary if there are large variations in surface slope within the averaging window [7]. Other methods such as the MUSIC algorithm should also be tested in order to speed up the computations [7].

We have also discussed basic effects to consider for coherence estimation. The performance of different interpolators regarding their effect on the degree of coherence were investigated and a cubic interpolator was found to perform satisfactory. It was also noted that the estimated degree of coherence is biased for small averaging windows. It is therefore important to chose a window that is large enough to minimise the bias effect and reduce the RMS error but small enough to avoid any extra decorrelation that is due to uncompensated topography. It is, in principle, possible to correct for the bias and arrive at a calibrated coherence value.

8. ACKNOWLEDGEMENT

The authors wish to acknowledge Patrick Svedjenäs for his assistance with the computer programming.

9. REFERENCES

[1] Graham L. C., "Synthetic interferometer radar for topographic mapping", *Proceedings of the IEEE*, 62, pp. 763-768, 1974.

[2] Wegmüller U., Werner C. L. & Rosen P. A., "Derivation of terrain slope from SAR interferometric phase gradient", *Proceedings of the second ERS-1 Symposium held in Hamburg*, ESA SP-361 II Space at the service of our environment, pp. 711-715, 1993.

[3] Werner C. L., Wegmüller U., Small D. L. & Rosen P. A., "Applications of interferometrically derived terrain slopes: normalization of SAR backscatter and the interferometric correlation coefficient", *Proceedings of the second ERS-1 symposium, Hamburg*, ESA SP-361 II Space at the service of our environment, pp. 723-726, 1993.

[4] Ulander L. M. H. & Hagberg J. O., "Use of INSAR for Radiometric Calibration over Sloping Terrain", *Proceedings of the CEOS SAR Calibration Workshop*, (held at ESTEC, Noordwijk, 20-24 Sept. 1993, ESA WPP-048, pp. 147-159, 1993.

[5] Ulander L. M. H., "Accuracy of using point targets for SAR calibration", *IEEE Transactions on Aerospace Electron. Syst.*, 27 (1), pp. 139-148, 1991.

[6] Gray A. L., Vachon P. W., Livingstone C. E. & Lukowski T. I., "Synthetic Aperture Radar Calibration using Reference Reflectors", *IEEE Transactions on Geoscience and Remote Sensing*, 28 (3), pp. 374-383, 1990.

[7] Boashash B., "Estimating and Interpreting the Intantaneous Frequency of a Signal – Part 2: Algorithms and Applications", *Proc. IEEE*, 80 (4), pp. 540-568, 1992.

[8] Rife D. C. & Boorstyn R. R., "Single Tone Parameter Estimation from Discrete-time Observations", *IEEE Trans. Inform. Theory*, 20, pp. 591-598, 1974.

[9] Born M. & Wolf E., "Principles of Optics", 6 ed. Pergamon Press, 1980.

[10] Zebker H. A. & Villasenor J., "Decorrelation of interferometric radar echos", *IEEE Transactions on Geoscience and Remote Sensing*, 30 (5), pp. 950-959, 1992.

[11] Hagberg J. O., Ulander L. M. H. & Askne J., "Repeat-Pass SAR Interferometry over Forested Terrain", *IEEE Transactions on Geoscience and Remote Sensing*, in press.